Solar Water Splitting To Generate Hydrogen Fuel: Photothermal Electrochemical Analysis

Stuart Licht†

Department of Chemistry and Institute of Catalysis, Technion Israel Institute of Technology, Haifa, 32000, Israel

Received: September 11, 2002; In Final Form: February 6, 2003

A novel model is derived for electrochemical solar water splitting processes by semiconductors, which is the first derivation of band gap restricted thermal enhanced solar water splitting efficiencies. The theory combines photodriven charge transfer, with excess subband gap insolation to lower the water potential, providing a process of highly efficient elevated temperature solar electrolysis of water to H_2 fuel. Solar water splitting can provide clean, renewable sources of H_2 fuel. Prior models had indicated only low conversion efficiencies would be attainable. A theoretical basis is developed for solar energy conversion efficiencies in the 50% range as determined for both AM0 and AM1.5 insolation with contemporary thermodynamic values over a wide range of temperature and pressure conditions. The temperature and pressure consistent for a range of systems with various minimum band gaps, $E_{g\,min}(T,p)$, are determined. At these values of T and p a photoelectonic conversion efficiency, η_{photo}, yields a solar energy conversion efficiency for water splitting of $\eta_{solar\,max}(T,p) = (1.229\ V)\eta_{photo}/E°_{H_2O}(T,p_{H_2O})$. At $p_{H_2O} = 1$ bar, values of $E°_{H_2O}$ include 1.229 V (25 °C), 1.167 V (100 °C), 1.116 V (300 °C), 1.034 V (600 °C), 0.919 V (1000 °C), and 0.771 V (1500 °C); at $p_{H_2O} = 500$ bar values of $E°_{H_2O}$ include 1.224 V (25 °C), 1.163 V (100 °C), 1.007 V (300 °C), 0.809 V (600 °C), and 0.580 V (1000 °C).

1. Introduction

The concept of utilizing driven water splitting to provide a H_2 fuel was suggested at least as early as the time of Jules Verne,[1] and H_2 propulsion for transportation is receiving increasing attention,[2] but what is to be the H_2 source? In principle, solar energy is sufficiently energetic to photodissociate water molecules, providing a clean, renewable source of H_2 fuel. The UV and visible energy rich portion of the solar spectrum is transmitted through H_2O. Therefore sensitization, such as via semiconductors, is required to drive the water-splitting process. Extensive research has been conducted on indirect and direct photothermal,[3,4] photosynthetic,[5] and photoelectrochemical[6] solar water splitting processes. Each of these previous approaches has limitations, and as summarized in Scheme 1 has exhibited a limited conversion of solar energy to H_2, with the best results achieved with photoelectrochemical, semiconductor photosensitizers. Solar photoelectrochemical attempts to split water utilized TiO_2[7] and InP[8] and also multiple band gap semiconducotors.[9,10] To date the highest efficiencies have been observed with multiple band gap semiconductor electrolysis cells sustaining over 18% solar energy conversion efficiency to H_2.[10]

As previously summarized, early photoelectrochemical models had incorrectly predicted only low solar water splitting conversion efficiencies, with a maximum of ∼15%, would be attainable.[10] This was recently shown to be improved to ∼30% solar water splitting model conversion efficiency by eliminating (i) the linkage of photo to electrolysis surface area, (ii) nonideal matching of photo and electrolysis potentials, and incorporating the effectiveness of contemporary (iii) electrolysis catalysts and (iv) efficient multiple band gap photosensitizers.[10] This advanced and earlier models did not incorporate either heat effects on (semiconductor) charge utilization or semiconductor effects on heat utilization. At high temperatures water (≫2000 °C) chemically disproportionates without electrolysis. However, catalysis, gas recombination, and containment materials limitations above 2000 °C have led to very low efficiencies.[4] Electrochemical water splitting, generating H_2 and O_2 at separate electrodes, largely circumvents the gas recombination limitations, and in particular, a hybrid of photothermal electrochemistry will be shown to provide a pathway for efficient solar energy utlization. Utilizing heat to facilitate water electrolysis had been suggested,[11] although no rigorous analysis from the fundamentals of solar energy, thermodynamics, and electrochemical processes had been developed.

In a recent letter, a novel model was introduced for electrochemical solar water splitting processes by semiconductor materials, which is the first derivation of band gap restricted, thermal enhanced solar water splitting efficiencies.[12] One schematic representation for this solar thermal water electrolysis assisted (photothermal electrochemical water splitting) is presented in Scheme 2, and rather than a field of concentrators, similar systems may use individual solar concentrators. This paper extends our theoretical derivation of band gap restricted, thermal enhanced solar water splitting efficiencies to additionally include supraatmosphere solar radiation (AM0 insolation), as well as conditions conducive to high pressure electrolyisis water splitting. Photodriven charge transfer through a semiconductor junction does not utilize photons that have energy below the semiconductor band gap. Hence, a silicon photovoltaic device does not utilize radiation below its band gap of ∼1.1 eV, while a AlGaAs/GaAs multiple band gap photovoltaic does not utilize radiation of energy less than the 1.43 eV band gap of GaAs. As will be shown, this unutilized, available long wavelength insolation represents a significant fraction of the solar spectrum. This long wavelength insolation can be filtered and used to heat water prior to electrolysis. The thermodynamics of heated water

† E-mail: chrlicht@techunix.technion.ac.il.

10.1021/jp026964p CCC: $25.00
Published on Web 04/11/2003

SCHEME 1: Solar Water Splitting Processes

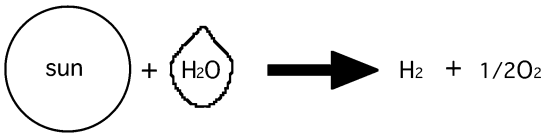

process	limitations, potential
photosynthetic, biological & photochemical	demonstrated efficiencies very low, generally < 1% solar energy conversion
photothermal, single step (direct)	gas recombination limitations, high temperature material limitations, generally < 1% solar energy conversion
photothermal, multistep	lower temp than single step, although stepwise reaction inefficiencies lead to losses, generally < 10% solar conversion
photoelectrochemical, *in* & *ex-situ*	10-20% solar energy conversion, *in-situ* interfacial instability limitations
photothermal electrochemical	theory was unavailable, potential for >> 20% solar conversion, requires solar concentration

SCHEME 2: Schematic Representations of Solar Water Electrolysis Improvement through Excess Solar Heat Utilization

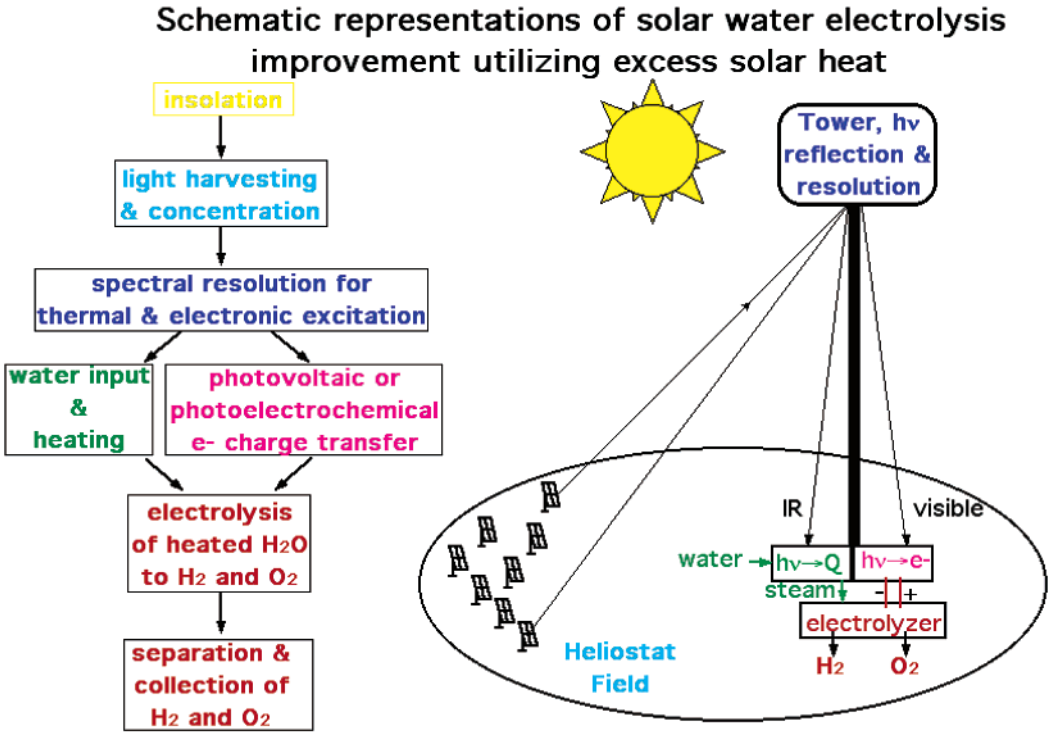

dissociation are more favorable than that at room temperature. This is expressed by a free energy chemical shift and a decrease in the requisite water electrolysis potential, which can considerably enhance solar water splitting efficiencies. A theoretical basis is developed for solar energy conversion efficiencies in the 50% range as determined with contemporary thermodynamic values, combining excess subband gap insolation with efficient photodriven charge transfer into highly efficient elevated temperature solar electrolysis of water to H_2 fuel.

2. Theory of Electrochemical Thermal Solar/H_2 Energy Conversion

The spontaneity of the H_2 generating water splitting reaction is given by the free energy of formation, ΔG°_f, of water and with the Faraday constant, F, the potential for water electrolysis:

$$H_2O \rightarrow H_2 + (1/2)O_2 \qquad (1)$$

$$-\Delta G^\circ_{split} = \Delta G^\circ_f(H_2O);$$
$$\Delta G^\circ_f(25\ ^\circ C, 1\ bar, H_2O_{liq}) = -237.1\ kJ\ mol^{-1} \quad (2)$$

$$E^\circ_{H_2O} = \Delta G^\circ_f(H_2O)/2F;$$
$$E^\circ_{H_2O}(25\ ^\circ C, 1\ bar, H_2O_{liq}) = 1.229\ V \quad (3)$$

Reaction 1 is endothermic, and electrolyzed water will cool unless external heat is supplied. The enthalpy balance and its related thermoneutral potential, E_{tneut}, are given by

$$-\Delta H_{split} = \Delta H_f(H_2O_{liq});$$
$$\Delta H^\circ_f(25\ ^\circ C, 1\ bar, H_2O_{liq}) = -285.8\ kJ\ mol^{-1} \quad (4)$$

$$E_{tneut} \equiv -\Delta H_f(H_2O_{liq})/2F;$$
$$E^\circ_{tneut}(25\ ^\circ C, 1\ bar, H_2O_{liq}) = 1.481\ V \quad (5)$$

The water electrolysis rest potential, eq 3, is determined from extrapolation to ideal conditions. Variations of the concentration, c, and pressure, p, from ideality are respectively expressed by the activity (or fugacity for a gas) as $a = \gamma c$ (or γp for a gas), with the ideal state defined at 1 atm for a pure liquid (or solid), and extrapolated from $p = 0$ or for a gas or infinite dilution for a dissolved species. The formal potential, measured under real conditions of c and p, can deviate significantly from the (ideal thermodynamic) rest potential; for example, the activity of water, a_w, at, or near, ambient conditions generally ranges from approximately 1 for dilute solutions to less than 0.1 for concentrated alkaline and acidic electrolytes.[13,14] The potential for the dissociation of water decreases from 1.229 V at 25 °C in the liquid phase to 1.167 V at 100 °C in the gas phase. Above the boiling the point, pressure is used to express the variation of water activity. The variations of the electrochemical potential for water in liquid and gas phase are given by

$$E(H_2O_{liq}) = E^\circ(H_2O_{liq}) + (RT/2F)\ln(\gamma_{H_2}p_{H_2}(\gamma_{O_2}p_{O_2})^{1/2}/a_w) \quad (6)$$

$$E(H_2O_{gas}) = E^\circ(H_2O_{gas}) + (RT/2F)\ln(\gamma_{H_2}p_{H_2}(\gamma_{O_2}p_{O_2})^{1/2}/\gamma_{H_2O}p_{H_2O}) \quad (7)$$

As noted in Table 1, the critical point of water is 374 °C and 221 bar. Below the boiling point, $E^\circ_{H_2O}$ is similar for 1 bar and high water pressure, but it diverges sharply above these conditions. Values of $E^\circ_{H_2O}$ include the following: at $p_{H_2O} = 1$ bar, 1.229 V (25 °C), 1.167 V (100 °C), 1.116 V (300 °C), 1.034 V (600 °C), 0.919 V (1000 °C), and 0.771 V (1500 °C); at $p_{H_2O} = 500$ bar, 1.224 V (25 °C), 1.163 V (100 °C), 1.007 V (300 °C), 0.809 V (600 °C), and 0.580 V (1000 °C). Due to overpotential losses, ζ, the necessary applied electrolysis potential is

$$V_{H_2O}(T) = E^\circ_{H_2O}(T) + \zeta_{anode} + \zeta_{cathode} \equiv (1 + \zeta)E^\circ_{H_2O}(T) \quad (8)$$

The water electrolysis potential energy conversion efficiency occurring at temperature, T, is $\eta_{echem}(T) \equiv E^\circ_{H_2O}(T)/V_{H_2O}(T)$. Solar water splitting processes utilize ambient temperature water as a reactant. An interesting case occurs if heat is introduced to the system, that is, when electrolysis occurs at an elevated temperature, T, using water heated from 25 °C. The ratio of the standard potential of water at 25 °C and T is $r = E^\circ_{H_2O}(25\ ^\circ C)/E^\circ_{H_2O}(T)$. As shown in Figure 1, $E^\circ_{H_2O}(T)$ diminishes with increasing temperature, as calculated using contemporary thermodynamic values summarized in Table 1.[15,16] In this case, an effective water splitting energy conversion efficiency of $\eta'_{echem} > 1$ can occur, to convert 25 °C water to H_2 by electrolysis at T:

$$\eta'_{echem} = r\eta_{echem}(T) = rE^\circ_{H_2O}(T)/V_{H_2O}(T) = E^\circ_{H_2O}(25\ ^\circ C)/V_{H_2O}(T) \quad (9)$$

For low overpotential electrolysis, $V_{H_2O}(T > 25\ ^\circ C)$ can be less than $E^\circ_{H_2O}(25\ ^\circ C)$, resulting in $\eta'_{echem} > 1$ from eq 9. Whether formed with pn or Schottky type junctions, the limiting, energetic constraints on photovoltaic (solid state) driven electrolysis are identical to those for photoelectrochemical water splitting, although the latter poses additional challenges of semiconductor/electrolyte interfacial instability, area limitations, catalyst restrictions, and electrolyte light blockage. The overall solar energy conversion efficiency of water splitting is constrained by the product of the available solar energy electronic conversion efficiency, η_{photo}, with the water electrolysis energy conversion efficiency.[10] For solar photo*thermal* water electrolysis, a portion of the solar spectrum will be used to drive charge transfer, and an unused, separate portion of the insolation will be used as a thermal source to raise ambient water to a temperature T:

$$\eta_{solar} = \eta_{photo}r\eta_{echem} = \eta_{photo}[E^\circ_{H_2O}(25\ ^\circ C)/E^\circ_{H_2O}(T)][E^\circ_{H_2O}(T)/V_{H_2O}(T)] = \eta_{photo}[1.229/V_{H_2O}(T)] \quad (10)$$

Conditions of $\eta_{solar} > \eta_{photo}$ will be shown to place specific restrictions on the photosensitizer. When $V_{H_2O} < E_{tneut}$, heat must flow to compensate cooling which occurs at the electrolysis rate; that is, for an enthalpy-balanced system any additional required heat must flow in a flux equivalent to $i_{heat} = i_{H_2O}$, and at an average power P_{heat}, such that

$$E_{tneut} = V_{H_2O} + P_{heat}/i_{H_2O} \quad (11)$$

A photoelectrolysis system can contain multiple photoharvesting units and electrolysis units, where the ratio of electrolysis to photovolatic units is defined as R. Efficient water splitting occurs with the system configured to match the water electrolysis and photopower maximum power point. This is illustrated in Figure 2 representing the photosensitizers as power supplies driving electrolysis with a photodriven charge from a photon flux to generate a current density (electrons per unit area) to provide the two stoichiometric electrons per split water molecule. For example, due to a low photopotential, a photodriven charge from three serial arranged Si energy gap devices may be required to dissocate a single room temperature water molecule, as described in the lower right portion of the figure. Alternately, as in a multiple band gap device such as AlGaAs/GaAs, the high potential of a single photodriven charge may be sufficient to dissocate two room temperature water molecules, as described in the upper right portion of the figure. In the figure, consider four different photoelectrolysis systems, each functioning at the same efficiency for solar conversion of electronic power, η_{photo}, and the same efficiency for solar conversion of thermal power, η_{heat}. Whereas the photoconverter in the first system generates the requisite water electrolysis potential, that in the second system generates twice that potential (albeit at

TABLE 1: Thermodynamic Free Energy and Enthalpy of Water Formation for (a) All Constituents at 1 bar and (b) 500 bar Water and 1 bar H_2 and O_2[a]

	(a) H_2, O_2, H_2O						(b) H_2O			
T (K)	P (bar)	state	P (bar)	state	$\Delta G°_f$ (kJ/mol H_2O)	$\Delta H°_f$ (kJ/mol H_2O)	P (bar)	state	$\Delta G°_f$ (kJ/mol H_2O)	$\Delta H°_f$ (kJ/mol H_2O)
298	1	gas	1	liquid	237.1	285.8	500	liquid	236.2	285.0
300	1	gas	1	liquid	236.8	285.8	500	liquid	235.9	285.0
373	1	gas	1	liquid	225.2	280.2				
373	1	gas	1	gas	225.2	239.5				
400	1	gas	1	gas	223.9	243.0	500	liquid	220.1	282.0
500	1	gas	1	gas	219.1	243.8	500	liquid	204.9	278.8
600	1	gas	1	gas	214.0	244.8	500	liquid	190.5	274.9
647	1	gas	1	gas			221	critical point		
700	1	gas	1	gas	208.8	245.7	500	supercritical	176.9	268.3
800	1	gas	1	gas	203.5	246.5	500	supercritical	164.6	258.1
900	1	gas	1	gas	198.1	247.2	500	supercritical	153.2	254.6
1000	1	gas	1	gas	192.6	247.9	500	supercritical	142.0	253.2
1100	1	gas	1	gas	187.0	248.4	500	supercritical	130.9	252.5
1200	1	gas	1	gas	181.4	248.9	500	supercritical	119.9	252.1
1300	1	gas	1	gas	175.7	249.4	500	supercritical	108.8	252.0
1400	1	gas	1	gas	170.1	249.9	500	supercritical	97.8	251.9
1500	1	gas	1	gas	164.4	250.2	500	supercritical	86.8	251.9
1600	1	gas	1	gas	158.6	250.5	500	supercritical	75.8	251.9
1700	1	gas	1	gas	152.9	250.8	500	supercritical	64.8	252.0
1800	1	gas	1	gas	147.1	251.1	500	supercritical	53.8	252.0
2300	1	gas	1	gas	118.0	252.1				
2800	1	gas	1	gas	88.9	252.8				
3300	1	gas	1	gas	59.6	253.5				
3800	1	gas	1	gas	30.3	254.2				
4310	1	gas	1	gas	0.0	255.1				

[a] The 1 bar values are calculated from data in ref 15, and the 500 bar values are from ref 16.

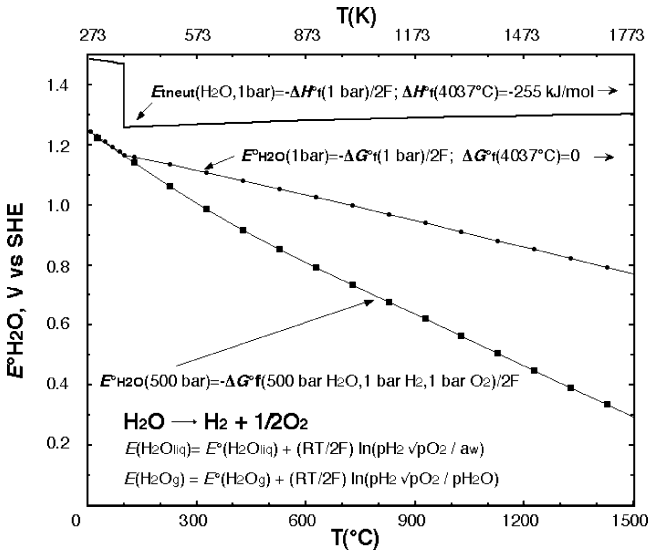

Figure 1. Thermodynamic and electrochemical values for water dissociation to H_2 and O_2 as a function of temperature. The curves without squares are calculated at 1 bar, for liquid water through 100 °C and for steam at higher temperatures. The high pressure utilized in this additional curve (p_{H_2O} = 500 bar; $p_{H_2} = p_{O_2}$ = 1 bar) is of general interest as (i) the electrolysis potential is diminished compared to that of water at 1 bar, and (ii) the density of the high-pressure fluid is similar to that the liquid and (iii) may be generated in a confined space by heating or electrolyzing liquid water.

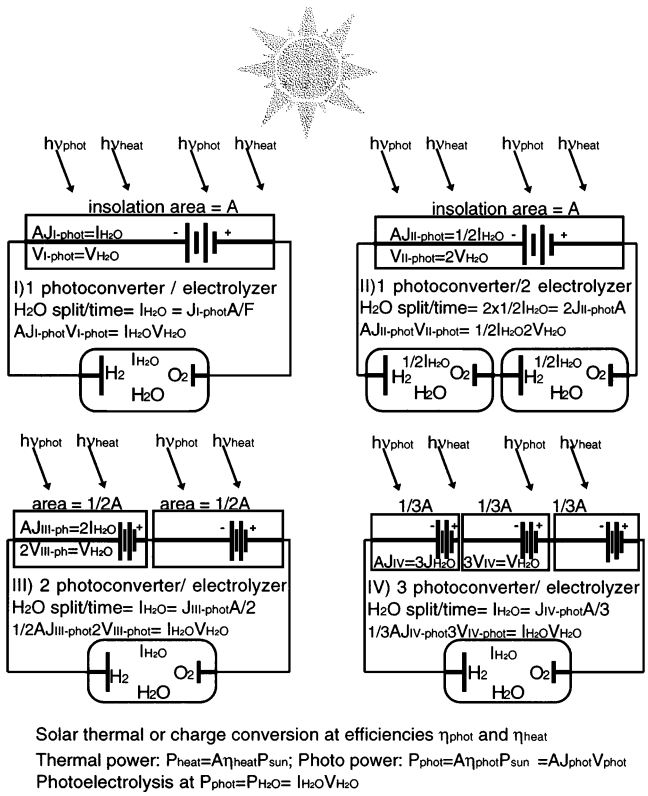

Figure 2. Alternate configurations varying the number of photoharvesting units and electrolysis units for solar water splitting. The photoconverter in the first system generates the requisite water electrolysis potential; that in the second system generates twice that potential, while the photoconverter in the third and fourth units generate respectively only one-half or one-third this potential.

one-half the photocurrent), while the photoconverters in the third and fourth units generate respectively only one-half or one-third this potential (albeit at 2-fold or 3-fold the photocurrent to retain the same efficiency). The harvested photon power for electronic energy per unit insolation area will be the same in each of the four cases. Furthermore, the number of harvested photons for thermal energy, and the total thermal power available to heat water, will be the same for the four cases. For example, in case II, although twice the number of electrolysis units are utilized, each operates at only half the hydrolysis current compared to cases I, III, and IV, splitting the same equivalents of water.

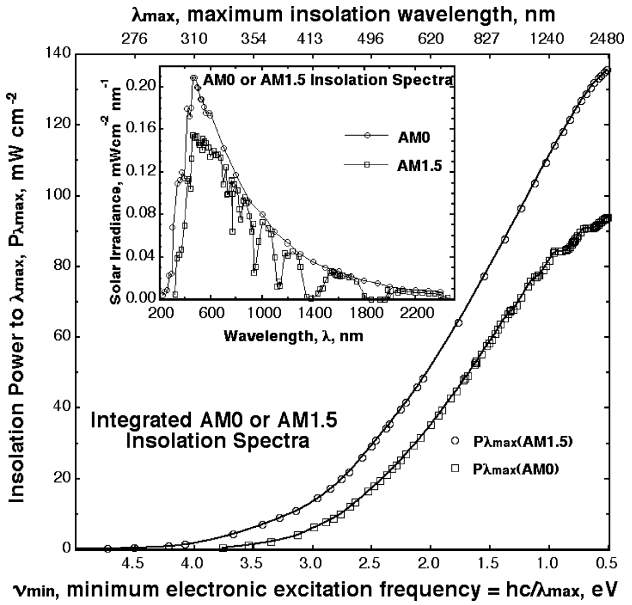

Figure 3. Solar irradiance (mW cm^{-2} nm^{-1}) in the figure inset, and total insolation power (mW cm^{-2}) of the solar spectrum in the main figure.

For solar-driven charge transfer, this maximum power is described by the product of the insolation power, P_{sun}, with η_{photo}, which is then applied to electrolysis, $\eta_{phot}P_{sun} = P_{echem} = i_{H_2O}V_{H_2O}$. Rearranging for i_{H_2O}, and substituting into eq 11, yields for heat balanced solar electrolysis at conditions of T and p, initiating at 25 °C and 1 bar water

$$E_{tneut} = 1.481\ \text{V} = V_{H_2O}(T,p)(1 + P_{heat}/\eta_{photo}P_{sun}) \quad (12)$$

Figure 3 presents the available insolation power, $P_{\lambda_{max}}$ (mW cm^{-2}), of the integrated solar spectrum up to a minimum electronic excitation frequency, ν_{min} (eV), determined by integrating the solar spectral irradiance, S (mW cm^{-2} nm^{-1}), as a function of a maximum insolation wavelength, λ_{max} (nm). This $P_{\lambda_{max}}$ is calculated for the conventional terrestial insolation spectrum either above the atmosphere, AM0, or through a 1.5 atm pathway, AM1.5. Relative to the total power, P_{sun}, of either the AM0 or AM1.5 insolation, the fraction of this power available through the insolation edge is designated $P_{rel} = P_{\lambda_{max}}/P_{sun}$. In solar energy balanced electrolysis, excess heat is available primarily as photons without sufficient energy for electronic excitation. The fraction of these subband gap photons in insolation is $\alpha_{heat} = 1 - P_{rel}$, and comprises an incident power of $\alpha_{heat}P_{sun}$.

Figure 4 presents the variation of the minimum electronic excitation frequency, ν_{min}, with α_{heat}, determined from P_{rel} using the values of $P_{\lambda_{max}}$ summarized in Figure 3. A semiconductor sensitizer is constrained not to utilize incident energy below the band gap. As seen in Figure 4 by the intersection of the solid line with ν_{min}, over one-third of insolation power occurs at $\nu_{min} < 1.43$ eV (867 nm), equivalent to the IR not absorbed by GaAs or wider band gap materials. The calculations are updated from our previous calculation[12] to include both the AM0 and AM1.5 spectra. In the relevant visible and IR range from 0.5 to 3.1 eV (±0.03 eV) for both the AM0 and AM1 insolation spectra, ν_{min} (α_{heat}) in the figure is well represented ($R^2 \geq 0.999$) by the polynomial fits:

$$\nu_{AM0}\ (\text{eV}) = 0.53008 + 3.1405\alpha_{heat} - 3.0687\alpha_{heat}^{\ 2} + 2.9103\alpha_{heat}^{\ 3} \quad (13)$$

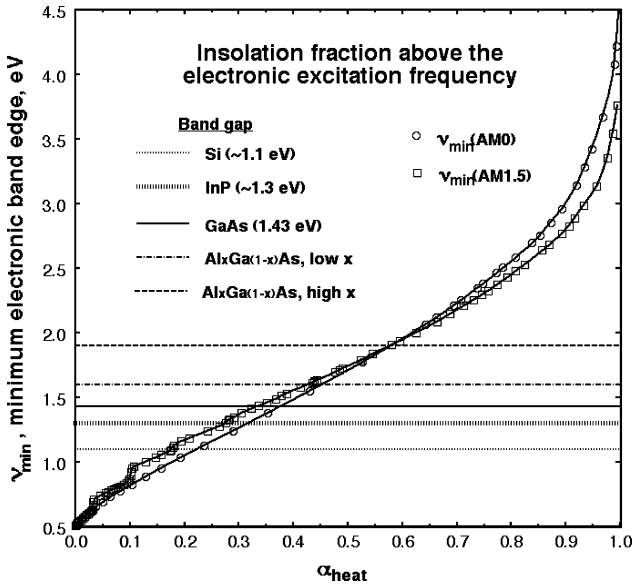

Figure 4. α_{heat}, the fraction of solar energy available below the minimum sensitizer insolation frequency used to drive charge transfer, ν_{min}. α_{heat} is determined as $1 - P_{rel}$, with $P_{rel} = P_{\lambda_{max}}/P_{sun}$, and using values of $P_{\lambda_{max}}$ summarized in Figure 3. The available incident power below ν_{min} will be $\alpha_{heat}P_{sun}$. The band gaps of various semiconductors are superimposed as horizontal lines in the figure.

$$\nu_{AM1.5}\ (\text{eV}) = 0.52827 + 4.0135\alpha_{heat} - 5.1286\alpha_{heat}^{\ 2} + 3.8980\alpha_{heat}^{\ 3} \quad (14)$$

When captured at a thermal efficiency of η_{heat}, the subband gap insolation power is $\eta_{heat}\alpha_{heat}P_{sun}$. Other available system heating sources include absorbed superband gap photons which do not effectuate charge separation, P_{recomb}, and noninsolation sources, P_{amb}, such as heat available from the ambient environment heat sink, and P_{recov}, such as heat recovered from process cycling or subsequent H_2 fuel utilization. The power equivalent for losses, such as the low power consumed in delivering the heated water to electrolysis, P_{pump}, can also be incorporated. Together these comprise the power for heat balanced electrolysis, which with P_{heat} from eq 12 yields α_{heat}:

$$P_{heat} = \eta_{heat}\alpha_{heat}P_{sun} + \beta; \quad \beta = P_{recomb} + P_{amb} + P_{recov} - P_{pump} \quad (15)$$

$$\alpha_{heat} = [\eta_{photo}/\eta_{heat}][\{(1.481\ \text{V})/(1 + \zeta)E^{\circ}_{H_2O}) - 1\} - \beta/(\eta_{heat}P_{sun}] \quad (16)$$

For solar electrolysis at T and p, a minimum insolation energy, ν_{min}, leaves available for transmittance the requisite thermal energy. This constrains the minimum electronic excitation energy and the band gap, $E_{g\,min}$, which is determined from eqs 13 and 14 using α_{heat} values estimated from eq 16:

$$E_{g\,min} = \nu_{min}(P_{sun},\alpha_{heat}); \quad \alpha_{heat}(T,p) \cong (\eta_{photo}/\eta_{heat})[((1.481\ \text{V})/E^{\circ}_{H_2O}(T,p)) - 1]$$

$$E_{g\,min}[(\text{AM0}),\ \text{eV}] = 0.53008 + 3.1405\alpha_{heat} - 3.0687\alpha_{heat}^{\ 2} + 2.9103\alpha_{heat}^{\ 3}$$

$$E_{g\,min}[(\text{AM1.5}),\ \text{eV}] = 0.52827 + 4.0135\alpha_{heat} - 5.1286\alpha_{heat}^{\ 2} + 3.8980\alpha_{heat}^{\ 3} \quad (17)$$

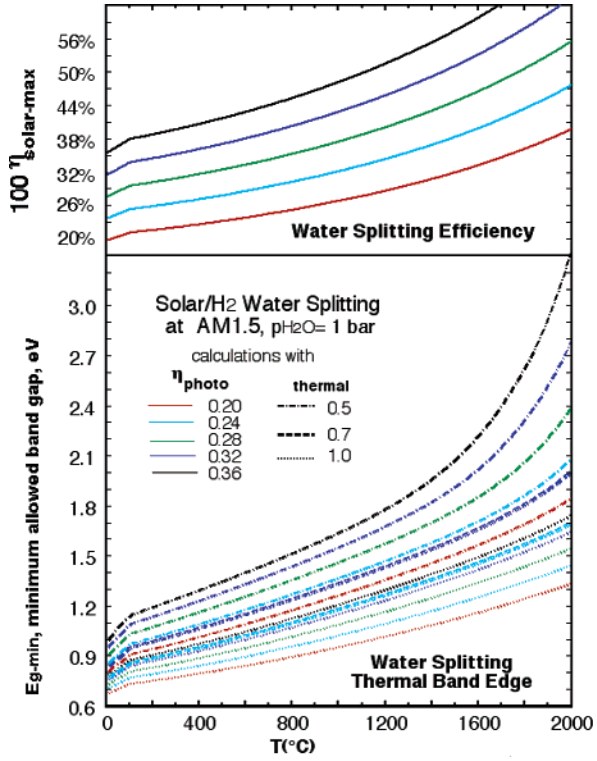

Figure 5. Energy conversion efficiency of solar-driven water splitting to generate H_2 as a function of temperature at AM1.5 insolation, with the system minimum band gap determined at $p_{H_2O} = 1$ bar. The maximum photoelectrolysis efficiency is determined from eq 18 for various indicated values of η_{photo}. The system minimum band gap is determined from eq 17 for various indicated values of η_{photo} and η_{heat}.

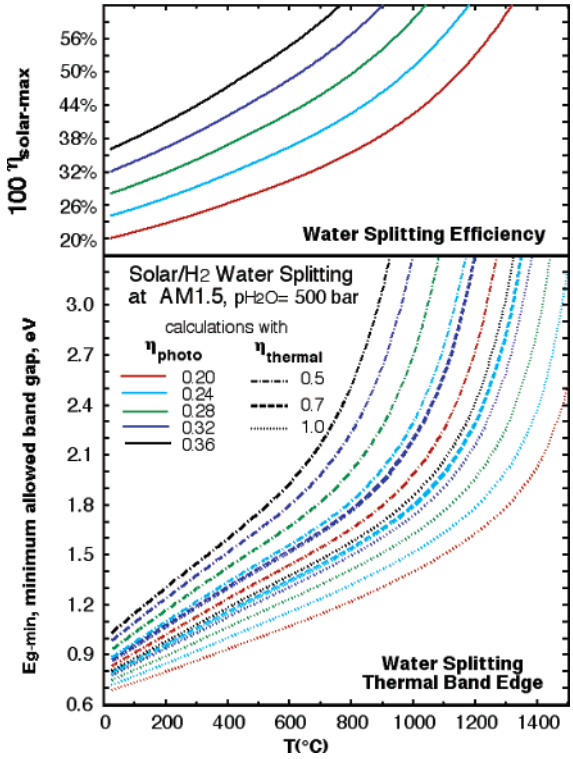

Figure 6. Energy conversion efficiency of solar-driven water splitting to generate H_2 as a function of temperature at AM1.5 insolation, with the system minimum band gap determined at $p_{H_2O} = 500$ bar. The maximum photoelectrolysis efficiency is determined from eq 18 for various indicated values of η_{photo}. The system minimum band gap is determined from eq 17 for various indicated values of η_{photo} and η_{heat}.

A value of $\zeta = 0$ will overestimate, and $\beta = 0$ will underestimate, α_{heat} in eq 16 as presented in eq 17. Contemporary commercial alkaline water electrolysis cells exhibit overall $\zeta \cong 0.15$,[17] and large surface area alkaline electrolysis cells sustain $\zeta < 0.05$.[10] Furthermore, ζ tends to diminish with increasing T, facilitating V_{H_2O} which approaches $E°_{H_2O}$ at elevated temperatures, and consistent with the rigorous upper limit for the solar electrolysis efficiency from eq 10:

$$\eta_{solar\ max}(T,p) = 1.229\eta_{photo}/E°_{H_2O}(T,p) \qquad (18)$$

In Figures 5−8, determinations of the solar water splitting energy conversion are summarized, as calculated from eq 18 using the $E°_{H_2O}(T,p)$ data in Figure 1, and the minimum allowed band gap, $E_{g\ min}(T,p)$ from eq 17 for a wide temperature range for various solar water splitting systems. Figures 5 and 6, or 7 and 8, are respectively modeled based on AM1.5, or AM0, insolation. Figures 5 and 7 are calculated, at various temperatures for $p_{H_2O} = 1$ bar, while Figures 6 and 8 repeat these calculations for $p_{H_2O} = 500$ bar. In Figure 6, compared to Figure 5, the rate of increase in temperature of $\eta_{solar\ max}$ is significantly greater for higher pressure photoelectrolysis ($p_{H_2O} = 500$ bar). However, as seen by comparing the minimum band gap in these figures (or in Figures 7 and 8 in the analagous AM0 models), at these higher pressures this higher rate of efficiency increase with temperature is offset by lower accessible temperatures (for a given band gap). A larger ζ in V_{H_2O} will diminish η_{solar}, but will extend the usable small band gap range. Together, Figures 5−8 determine the constraints on η_{solar} from various values of η_{photo}. The high end of contemporary experimental high solar conversion efficiencies ranges from 100% η_{photo} = 19.8% for multicrystalline single junction photovoltaics, to 27.6% and 32.6% for single junction and multiple junction photovoltaics.[18] The efficiency of solar thermal conversion tends to be higher, than solar electrical conversion, η_{photo}, particularly in the case of the restricted spectral range absorption used here; values of $\eta_{heat} = 0.5$, 0.7, or 1 are utilized for eq 17. While a small band gap, $E_g < 1.23$ eV, is insufficient for water cleavage at 25 °C, its inclusion in Figures 5−8 is of relevance in two cases: (i) where high temperature decreases $V_{H_2O}(T)$ below E_g and (ii) where this E_g is part of a multiple band gap sensitization contributing a portion of a larger overall photopotential. It is also noted that $E_g > 3.0$ eV is inadequate for an efficient use of the solar spectrum.

3. Solar/H_2 Electrochemical Thermal Conversion Efficiencies

Representative results from Figure 5 for solar water splitting to H_2 systems from AM1.5 insolation include a 50% solar energy conversion for a photoelectrolysis system at 638 °C with $p_{H_2O} = 500$ bar, $p_{H_2} = 1$ bar, and η_{photo}= 0.32. However, this high H_2O partial pressure system requires separation of a low partial pressure of H_2. Efficient photoelectrolysis is also determined for high relative H_2, such as for systems of $p_{H_2} = p_{H_2O} = 1$ bar, $\eta_{heat} = 0.7$, and $E_{g\ min} = E_g$(GaAs) =1.43 eV, in which efficiencies improve in Figure 5 from 28% (at 25 °C) to 42% at 1360 °C, or from 32% (25 °C) to 46% at 1210 °C, or from 36% (25 °C) to 49% at 1060 °C. The case of the GaAs band gap is of interest, as efficient multiple band gap photovoltaics have also been demonstrated using GaAs as the semiconductor minimum band gap component. ζ generated electrolysis heat is intrinsic to V_{H_2O} and will diminish η_{solar}, but will extend the small band gap range, $E_{g\ min}$. Consistent with the larger heat available up to $\alpha_{heat} = 0.6$ in Figure 4, moderately

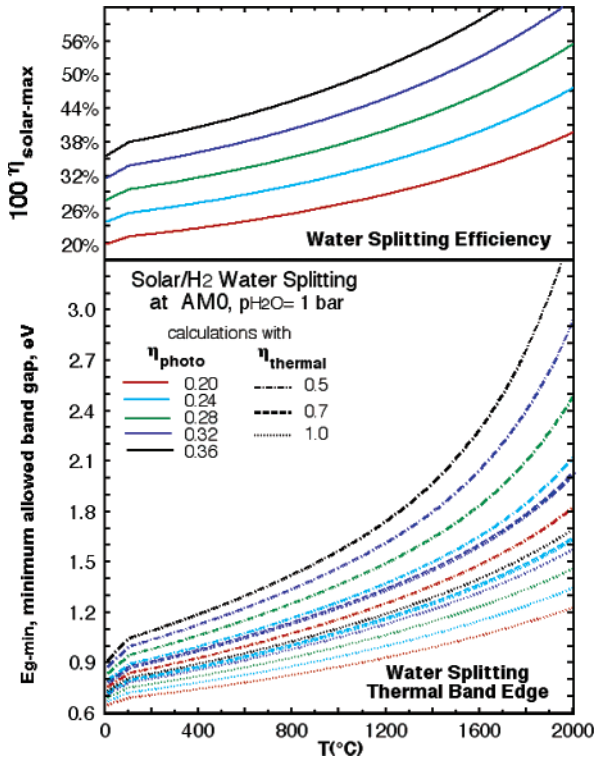

Figure 7. Energy conversion efficiency of solar-driven water splitting to generate H_2 as a function of temperature at AM0 insolation, with the system minimum band gap determined at $p_{H_2O} = 1$ bar. The maximum photoelectrolysis efficiency is determined from eq 18 for various indicated values of η_{photo}. The system minimum band gap is determined from eq 17 for various indicated values of η_{photo} and η_{heat}.

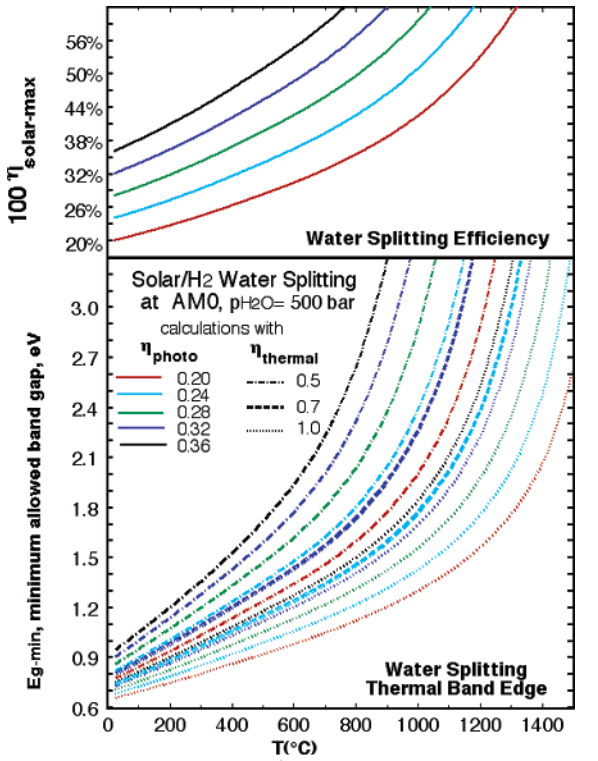

Figure 8. Energy conversion efficiency of solar-driven water splitting to generate H_2 as a function of temperature at AM0 insolation, with the system minimum band gap determined at $p_{H_2O} = 500$ bar. The maximum photoelectrolysis efficiency is determined from eq 18 for various indicated values of η_{photo}. The system minimum band gap is determined from eq 17 for various indicated values of η_{photo} and η_{heat}.

higher temperatures are accessible for fixed values of $E_{g\,min}$ with AM0 in Figures 7 and 8, compared to AM1.5 insolation in Figures 5 and 6.

4. Experimental Solar/H_2 Electrochemical Thermal Components

Experimentally, we have achieved $\eta_{solar} > 0.18$, using an $\eta_{photo} = 0.20$ AlGaAs/Si system,[10] as summarized in Figure 9 and still without inclusion of high temperature effects. Existing, higher η_{photo} (=0.28−0.33) systems should achieve proportionally higher results, and inclusion of heat effects and the elevated temperature decrease of the water electrolysis potential will lead to even higher values of solar energy to H_2 fuel conversion efficiencies. Thermally assisted solar electrolysis consists of (i) light harvesting; (ii) spectral resolution of thermal (subband gap) and electronic (superband gap) radiation, the latter of which (iiia) drives photovoltaic or photoelectrochemical charge transfer $V(i_{H_2O})$, while the former (iiib) elevates water to temperature, T, and pressure, p; and finally (iv) $V(i_{H_2O})$ driven electrolysis of $H_2O(T,p)$ as schematized in Scheme 2.

Experimental components for efficient solar-driven generation of H_2 fuel at 40−50% solar energy conversion efficiencies appear to be technologically available. In the 50% efficiency range photoelectrochemical cells tend to be unstable, which is likely to be exacerbated at elevated temperatures, and the model system will be particularly conducive to photovoltaic, rather than photoelectrochemical, driven electrolysis as previously compared in section 2. The photovoltaic component is used for photodriven charge into the electrolysis component, but does not contact the heated electrolyte. In this case the high efficiencies appear accessible, stable photovoltaics are commonly driven with concentrated insolation,[18] and specific to the system model here, heat will be purposely filtered from the insolation prior to incidence on the photovoltaic component.

Dielectric filters used in laser optics split insolation without absorption losses. For example, in a system based on a parabolic concentrator, a cassegrain configuration may be used, with a mirror made from fused silica glass with a dielectric coating acting as a band-pass filter. The system will form two focal spots with different spectral configurations: one at the focus of the parabola and the other at the focus of the cassegrain.[19] The thermodynamic limit of concentration is 46000 suns, the brightness of the surface of the sun. In a medium with refractive index greater than 1, the upper limit is increased by 2 times the refractive index, although this value is reduced by reflective losses and surface errors of the reflective surfaces, the tracking errors of the mirrors, and dilution of the mirror field. Specifically designed optical absorbers, such as parabolic concentrators or solar towers, can efficiently generate a solar flux with concentrations of ∼2000 suns, generating temperatures in excess of 1000 °C.[20,21]

Commercial alkaline electrolysis occurs at temperatures up to 150 °C and pressures to 30 bar,[17] and supercritical electrolysis occurs to 350 °C and 250 bar.[22] Although less developed than their fuel cell counterparts which have 100 kW systems in operation and developed from the same oxides,[23] zirconia and related solid oxide based electrolytes for high temperature steam electrolysis can operate efficiently at 1000 °C,[24,25] and approach the operational parameters necessary for efficient solar-driven water splitting. Efficient multiple band gap solar cells absorb light up to the band gap of the smallest band gap component. Thermal radiation is assumed to be split off (removed and utilized for water heating) prior to incidence on the semiconductor and hence will not substantially effect the band gap. Highly

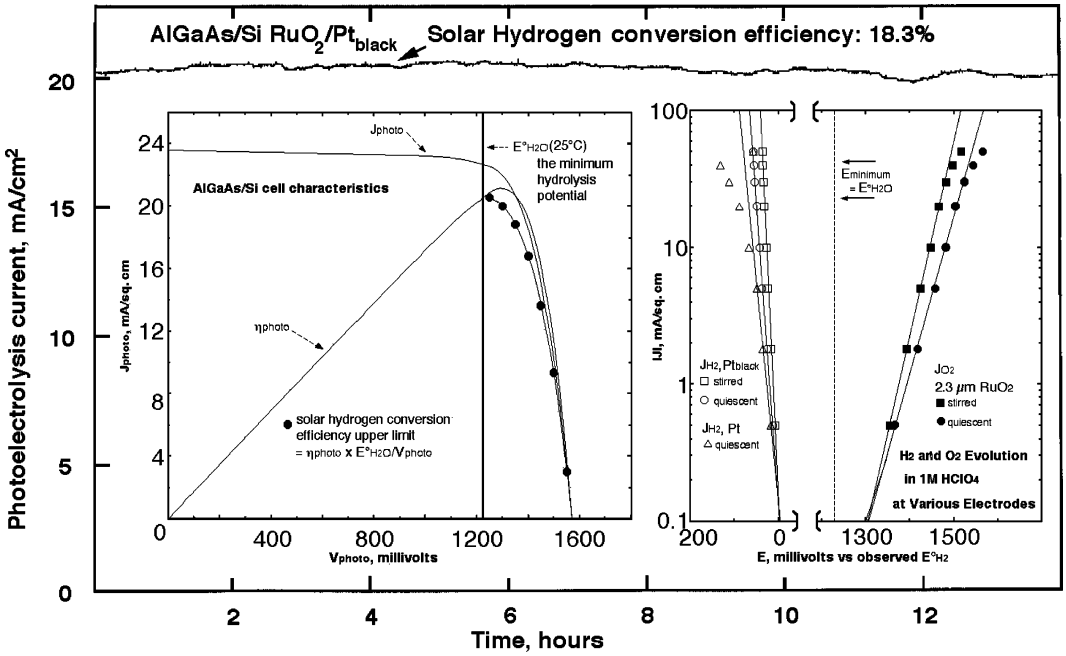

Figure 9. Measured water electrolysis current of the photoelectrolysis AlGaAs/Si RuO_2/Pt_{black} cell. Extended experimental details are provided in ref 10. Left inset: Current−voltage characteristics of the AlGaAs/Si cell. $\eta_{photo} = 100\%(J_{photo}V_{photo})/P_{illumination}$. Using the indicated, measured η_{photo} and V_{photo}, the upper limits of photoelectrolysis efficiency are calculated as $\eta_{photo}[(1.229\ V)/V_{photo}]$. Right inset: Potential variation with galvanostatic current density at various H_2 or O_2 electrodes in 1 M $HClO_4$. The O_2 electrode is 2.3 μm thick RuO_2. The H_2 electrodes are either Pt_{black} or planar Pt.

efficient photovoltaics have been demonstrated at a solar flux with a concentration of several hundred suns. AlGaAs/GaAs has yielded at η_{photo} an efficiency of 27.6%, and a GaInP/GaAs cell 30.3% at 180 suns concentration, while GaAs/Si has reached 29.6% at 350 suns, InP/GaInAs 31.8%, and GaAs/GaSb 32.6% with concentrated insolation.[18]

Solar energy driven water splitting combines several attractive features for energy utilization. The energy source (sun) and reactive media (water) for solar water splitting are readily available and are renewable, and the resultant fuel (generated H_2) and its discharge product (water) are each environmentally benign. The model presented here provides theoretical evidence that the combination of contemporary efficient multiple band gap photovoltaics and concentrated excess subband gap heat will combine into highly efficient elevated temperature solar electrolysis of H_2 fuel. Efficiency will be further enhanced by excess superband gap and nonsolar sources of heat, but diminished by losses in polarization and photoelectrolysis power matching. Solar concentration can provide the high temperature and diminish the requisite surface area of efficient electrical energy conversion components, and high temperature electrolysis components are available. The theory and initial results presented provide evidence that their combination into highly efficient solar generation of H_2 will be attainable.

Acknowledgment. This work was supported in part by the BMBF, the Lower Saxony−Israeli Joint Research Fund, and the GM Foundation.

References and Notes

(1) Nicholson and Carlisle first generated H_2 and O_2 by water electrolysis in 1800, and in 1874 J. Verne wrote "Water decomposed into its primitive elements, and decomposed doubtless by electricity, which will then have become a powerful and manageable force ... Yes, my friends, I believe that water will someday be employed as fuel, that hydrogen and oxygen, which constitute it, used singly or together, will furnish an inexhaustible source of heat and light ... I believe, then, that when the deposits of coal are exhausted, we shall heat and warm ourselves with water. Water will be coal of the future." From: Verne, J. *The Mysterious Island*; France, 1874.

(2) Kruger, P. *Int. J. Hydrogen Energy* **2001**, *26*, 1137.

(3) Funk, *Int. J. Hydrogen Energy* **2001**, *26*, 185.

(4) Kogan, A.; Spiegler, E.; Wolfshtein, M. *Int. J. Hydrogen Energy* **2000**, *25*, 739.

(5) Miyake, J.; Miyake, M.; Adsada, Y. *J. Biotechnology* **1999**, *70*, 89.

(6) *Semiconductor Electrodes and Photoelectrochemistry*; Licht, S., Ed.; Wiley−VCH: Weinheim, 2002.

(7) (a) Fujishima, A.; Honda, K. *Nature* **1972**, *238*, 37. (b) Zou, Z.; Ye, Y.; Sayama, K.; Arakawa, H. *Nature* **2001**, *414*, 625.

(8) Heller, A.; Asharon-Shalom, E.; Bonner, W. A.; Miller, B. *J. Am. Chem. Soc.* **1982**, *104*, 6942.

(9) Khaselev, O.; Turner, J. A. *Science* **1998**, *280*, 425.

(10) (a) Licht, S. *J. Phys. Chem. B* **2001**, *105*, 6281. (b) Licht, S.; Wang, B.; Mukerji, S.; Soga, T.; Umeno, M.; Tributsch, H. *J. Phys. Chem. B* **2000**, *104*, 8920.

(11) Bockris, J. O'M. *Energy Options*: Halsted Press: New York, 1980.

(12) Licht, S. *Electrochem. Commun.* **2002**, *4*, 789.

(13) Licht, S. *Anal. Chem*. **1985**, *57*, 514. Light, T. S.; Licht, S. *Anal. Chem.* **1987**, *59*, 2327.

(14) Licht, S. *Analysis in Highly Concentrated Solutions: Potentiometric, Conductance, Evanescent, Densometric, and Spectroscopic Methodologies*; Bard, A., Rubinstein, I., Eds.; Electroanalytical Chemistry 20; Marcel Dekker: New York, 1998; pp 87−140,

(15) Chase, M. W. *J. Phys. Chem. Ref. Data* **1998**, *14*, Monograph 9 (JANF Thermochemical Tables, 4th ed.).

(16) Chase, M. W. *J. Phys. Chem. Ref. Data* **1986**, Suppl. nos. 1−14 (JANF Thermochemical Tables, 3rd ed.).

(17) Kreuter, W.; Hofmann, H. *Int. J. Hydrogen Energy* **1998**, *23*, 661.

(18) Green, M. A.; Emery, K.; King, D. L.; Igari, S.; Warta, W. *Prog. Photovolt.* **2001**, *9*, 49.

(19) Yogev, A. Quantum Processes for Solar Energy Conversion; *Weizmann Sun Symp. Proc*., Rehovot, Israel, 1996.

(20) Karni, J.; Kribus, R.; Rubin, P.; Doron, *J. Sol. Energy Eng*. **1998**, *120*, 85.

(21) Segal, E.; Epstein, M. *Sol. Energy* **2000**, *69*, 229.

(22) Misch, B.; Firus, A.; Brunner, G. *J. Supercrit. Fluids* **2000**, *17*, 227.

(23) Yamamoto, O.; et al. *Electrochim. Acta* **2000**, *45*, 2423.

(24) Kusunoki, D.; et al. *Int. J. Hydrogen Energy* **1995**, *20*, 831.

(25) Eguchi, K.; Hatagishi, T.; Arai, H. *Solid State Ionics* **1996**, *86−8*, 1245.